Contrasting Ferromagnetism in Pyrite FeS₂ Induced by Chemical Doping versus Electrostatic Gating

Ezra Day-Roberts, ¹ Turan Birol, ² and Rafael M. Fernandes ¹

¹School of Physics and Astronomy, University of Minnesota, Minneapolis, MN 55455, USA

²Department of Chemical Engineering and Materials Science,
University of Minnesota, Minneapolis, Minnesota 55455, USA

Recent advances in electrostatic gating provide a novel way to modify the carrier concentration in materials via electrostatic means instead of chemical doping, thus minimizing the impurity scattering. Here, we use first-principles Density Functional Theory combined with a tight-binding approach to compare and contrast the effects of electrostatic gating and Co chemical doping on the ferromagnetic transition of FeS₂, a transition metal disulfide with the pyrite structure. Using tight-binding parameters obtained from maximally-localized Wannier functions, we calculate the magnetic susceptibility across a wide doping range. We find that electrostatic gating requires a higher electron concentration than the equivalent in Co doping to induce ferromagnetism via a Stoner-like mechanism. We attribute this behavior to the formation of a narrow Co band near the bottom of the conduction band under chemical doping, which is absent in the electrostatic gating case. Our results reveal that the effects of electrostatic gating go beyond a simple rigid band shift, and highlight the importance of the changes in the crystal structure promoted by gating.

I. INTRODUCTION

Transition metal disulfides, (TM)S₂, with the pyrite structure host a wide variety of electronic ground states [1]. Varying the transition metal TM tunes the band filling over a wide range, from a $3d^5$ electronic configuration in the case of MnS_2 to a $3d^{10}$ configuration for ZnS₂. As the carrier concentration changes, a rich landscape of electronic states emerges, including: an antiferromagnetic insulator (MnS₂)[2-4], a semiconductor (FeS_2) [5, 6], a ferromagnetic metal (CoS_2) [5, 6], an antiferromagnetic Mott insulator (NiS₂) [7–9], a superconductor (CuS_2) [10, 11], and another semiconductor (ZnS₂) [12]. Tuning continuously across these phases would provide a unique avenue to elucidate the interplay between different electronic orders. While it is possible to use chemical doping to move across most of the transition metal disulfides' phase diagram, this approach introduces disorder and local inhomogeneity, which complicates the theoretical picture [13].

Electrostatic gating offers a promising alternative to chemical doping as a means to tune the carrier concentration, while avoiding the steric and chemical (electronegativity, etc.) effects associated with the addition of dopants. While the effects achievable using a conventional gate dielectric are often limited, novel gating approaches such as using a polar oxide or ferroelectric gating are quite promising [14, 15]. Also exciting are the recent advances in electrostatic gating with ionic liquids or gels, which provide access to much higher electron concentrations than those attainable by dielectricbased gating [13, 16, 17], opening new avenues to explore different regions of electronic phase diagrams [18– 21], including wide regions of the disulfide pyrite electrondensity phase diagram. Indeed, in dielectric-based gating devices, breakdown voltages restrict the added carrier densities to values $< 10^{12} - 10^{13} \text{cm}^{-2}$ [13]. In contrast, the ability to achieve carrier concentrations of up to $8 \times 10^{14} \text{cm}^{-2}$ [22] via electrolyte gating has been widely employed to study a variety of phenomena in oxides, such as the structural transformation in VO₂ [23–25], the metal-insulator transition in SrRuO₃ [26, 27], and superconductor-insulator transitions in multiple materials [19, 28–31]. These studies, however, revealed an important issue associated with electrolyte gating: often, electrochemical effects beyond simple electrostatics are at play [16, 32–34]. For example, in $La_{0.5}Sr_{0.5}CoO_{3-\delta}$, oxygen vacancies are formed under positive gating voltages [35]. These vacancies, which are formed in response to gating, enhance the sensitivity of the electronic structure to gating. However, they also introduce a significant degree of irreversibility. While this irreversibility can be undesirable for certain applications, many attempts have been made to take advantage of these electrochemical effects for many applications as well [35-39]. In contrast to oxides, strong sulfur-sulfur bonding in the pyrite structure [40] makes the formation energy of single sulfur vacancies prohibitely high [41] while multi-vacancy defect complexes dominate the electrochemical response [42]. How these defect complexes diffuse and determine the electrochemical response in pyrites is far from clear.

Among the pyrite transition metal disulfides, FeS₂ has attracted interest both as a potential photovoltaic material, characterized by a high optical absorption, a low toxicity and a low cost to manufacture [43–45], and as a metallic ferromagnet when doped with cobalt [6, 46]. FeS₂ is often unintentionally doped, and a great amount of work has been performed on the nature of native dopants [41, 47] as well as the role of surface vs. bulk conduction [48, 49]. While the "doping puzzle" about the nature of native dopants in single crystals vs. films of FeS₂ seems to be resolved [42, 50], there are several open questions about the electronic properties of FeS₂ that remain unsettled, such as the impact of the conducting surface states [51], the nature of the ferromagnetic tran-

sition in the doped compounds [52], and the role of Co doping in inducing ferromagnetism even at very small doping concentrations [53].

To shed new light on some of these issues, in this paper we perform a first-principles study of electrostatically gated FeS₂ and CoS₂ with pyrite structure, systematically comparing their electronic and magnetic properties with those of chemically doped $Fe_{1-x}Co_xS_2$. To model electrostatic gating, we go beyond the rigid-band shift paradigm and account for changes in the band structure and in the crystal structure arising from the change in the carrier concentration [54]. By computing the magnetization, we find that ferromagnetism appears for a smaller added carrier concentration in the case of chemical doping as compared to electrostatic gating. We attribute this behavior to the different energy ranges of the wide sulfur anti-bonding band in the two cases, as well as to the existence of a narrow Co band near the bottom of the conduction band in the case of chemical doping.

By comparing the carrier-concentration evolution of the magnetization with that of the density of states, we propose that the ferromagnetism is promoted by the Stoner mechanism. This naturally accounts for the sensitivity of the ferromagnetism to the changes in the band structure caused by chemical doping and electrostatic gating. We go beyond the first-principles analysis by computing the Lindhard function from a multi-orbital tight-binding model derived from the maximally localized Wannier functions. We find that the non-interacting magnetic susceptibility is peaked at the Γ point of the Brillouin zone, confirming the Stoner-character of the ferromagnetic instability and ruling out finite wave-vector magnetic states.

The paper is organized as follows: In section II we summarize our methods. In section III we present our first-principles results on the magnetic, electronic, and crystalline structures of the chemically doped and electrostatically gated cases. In section IV we fit a tight binding model to our first-principles results to calculate the non-interacting magnetic susceptibility. We conclude with a summary of our main results in section V.

II. METHODS

DFT+U calculations were done using the VASP implementation of the projector-augmented-wave (PAW) approach [55, 56]. The exchange-correlation functional was approximated using the PBEsol set generalized gradient approximation (GGA), which is developed for accuracy in crystal structure relaxations [57]. To correct the underestimation of on-site interactions between electrons, DFT+U approach was used [58]. A value of U=5 eV was selected as a compromise to achieve good agreement with the experimental lattice constant and sulfur-sulfur distance for both FeS₂ and CoS₂ (see Supplemental Information). For FeS₂ alone, a lower value of approximately 2 eV is optimal, in agreement with previous works [59].

For CoS_2 alone, a much larger value of U is preferred, because the lattice constant is underestimated and the sulfur-sulfur distance is overestimated for all values below 7 eV. The U value of 5 eV gives an error in each lattice constant of less than 1% and an error in the sulfur-sulfur distance of about 2.5%. A Γ -centered k-point grid of $8 \times 8 \times 8$ was used for structural calculations along with a plane wave cutoff of 500 eV.

Structural parameters for chemically doped and electrostatically gated systems are determined by performing structural relaxations. These calculations allow spinpolarization to reflect the presence of local moments, which is important for obtaining realistic crystal structures in DFT. All further calculations are done without spin-polarization. Undoped FeS₂ is found to not be spin polarized in its ground state while for all other chemical doping levels the ground state is found to be spin polarized, consistent with previous reports [60, 61]. A tightbinding model is constructed by calculating the Maximally Localized Wannier Functions by employing the wannier90 package [62]. The Wannierization calculation is done in the non-spin polarized state with the same value of U, since we are concerned with the emergence of the magnetic instability and not with the behavior of the materials in their ferromagnetic state.

In order to compare the effects of electrostatic gating with chemical doping we performed two sets of calculations. To simulate electrostatic gating (EG) we consider undoped FeS₂ (or CoS₂) and vary the total number of electrons in the unit cell by adding electrons (or holes) [63]. The highest level of EG we considered was 1 removed electron or 0.5 added electrons per transition metal atom. This is almost an order of magnitude larger than the experimentally achievable values, and leads to very large changes in the crystal structure. Thus, the results presented for the highest levels of EG serve just to illustrate trends for comparison with chemical doping. To simulate chemical doping (CD), we replaced one, two, or three of the Fe ions in the unit cell with Co ions, corresponding to $x = 0.25, 0.50, \text{ and } 0.75 \text{ in } \text{Fe}_{1-x}\text{Co}_{x}\text{S}_{2}.$ For each different carrier concentration in EG we fully relaxed both the ionic positions and the lattice vectors. For the CD configurations, the dopants break the symmetry of the crystal structure, so cell shape distortions away from cubic are in principle permitted by symmetry. Since the average structure with disorder has cubic symmetry, such distortions were not allowed in our calculations. This was achieved by iteratively relaxing cell size and ionic positions separately until convergence was obtained.

The entire conduction band manifold that consists of $2 e_g$ orbitals and 1 sulfur anti-bonding orbital per FeS₂ formula unit was used for wannierization. This manifold is isolated from other bands so no disentanglement was necessary [64]. The tight binding models we obtained from the wannierization procedure reproduce the DFT band structure extremely well (see the supplemental materials for details), but this requires using a very large

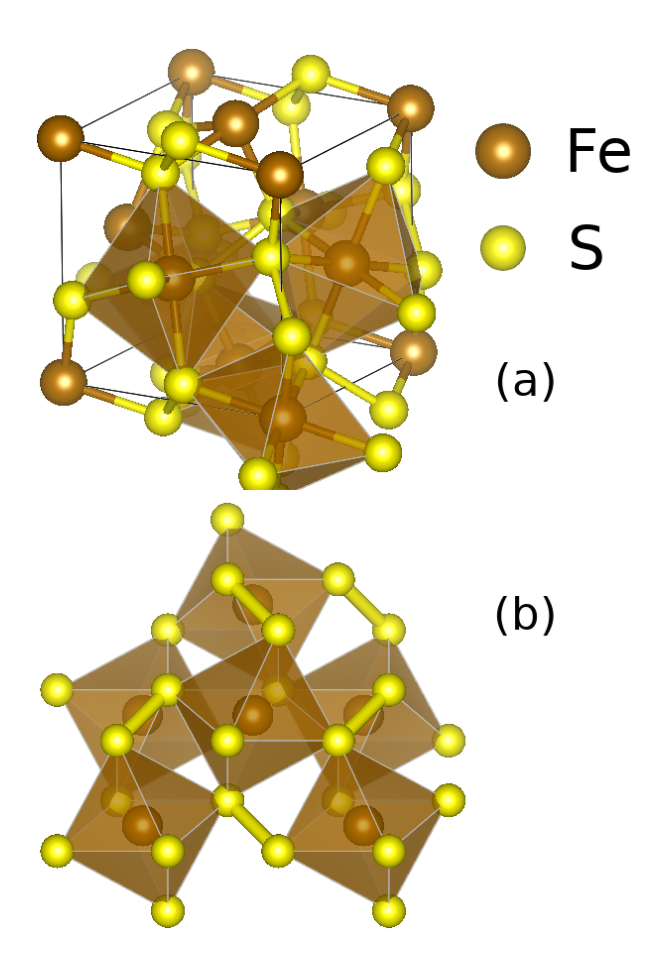


FIG. 1. (a) The simple-cubic primitive unit cell of FeS₂. The transition metal atoms occupy the corners and the face centers of this cell. Each transition metal atom is in the center of a sulfur octahedron. (b) The transition metal octahedra are corner sharing in the pyrite structure. In addition, every sulfur is part of a dimer connecting neighboring octahedra.

	Lattice Constant (Å)	Internal parameter (u)
$FeS_2 Exp$	5.428	0.385
FeS ₂ Theory	5.421	0.387
CoS ₂ Exp	5.535	0.395
CoS_2 Theory	5.510	0.391

TABLE I. Experimental crystal structure parameters for pure FeS_2 and CoS_2 compared with our calculations [65, 66].

number of hopping parameters. As a result, we do not report our hopping parameters.

III. FIRST-PRINCIPLE RESULTS

A. Magnetization

The pyrite structure has a simple cubic cell, consisting of a face-centered lattice of transition metal atoms each surrounded by a distorted sulfur octahedron (see Fig. 1).

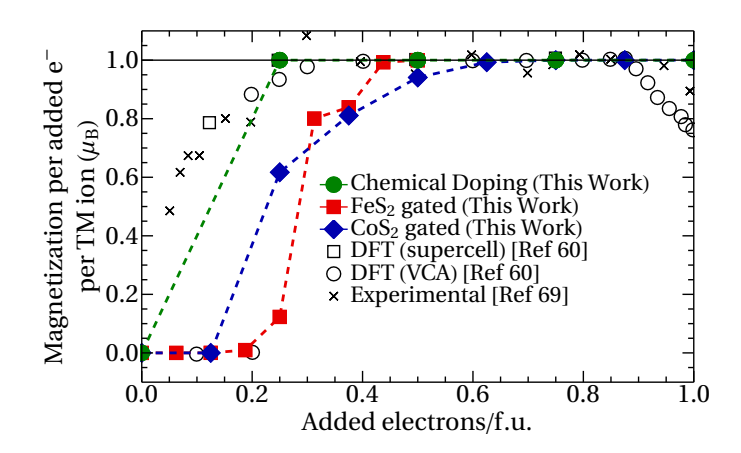


FIG. 2. Magnetization per added free electron as function of the number of added electrons. Our DFT+U results are compared with previous first-principles and experimental results on doped $\rm Fe_{1-x}Co_xS_2$ [60]. Note that electrostatically gated systems do not achieve 100% spin polarization until approximatelly 0.4 electrons are added to FeS2. Furthermore, electrostatic gating requires a higher added electron concentration to achieve ferromagnetism as compared to chemical doping.

The sulfur atoms form covalently bonded dimers, with the center point of the dimers forming another FCC lattice shifted from the transition metal lattice by half a lattice vector [67]. Because the sulfur atoms share two electrons in these dimers, the sulfur charge state is -1. This results in a total charge of -2 per dimer, and hence the iron atoms have an Fe²⁺ valence. This is in contrast to oxides and most other transition metal dichalcogenides where the chalcogens have a -2 charge, implying an Fe⁴⁺ valence [68]. In FeS₂, the dimer anti-bonding states are unoccupied and overlap with the empty Fe e_q bands. These dimers are thus an important ingredient of the electronic structure. The sulfur-sulfur distance controls the energy of the sulfur anti-bonding bands that make up the bottom of the conduction band in FeS_2 . There is only one internal crystallographic parameter, u, which controls the sulfur atoms' positions at (u, u, u) and at the symmetry-equivalent positions. This parameter controls both the distortion of the octahedra and the relative sulfur-sulfur and transition metal-sulfur distances. Table I lists the previously reported experimental lattice constant and internal parameter [65, 66], comparing them to the relaxed values found in this work. The discrepencies come from our choice to use a single value of U for both FeS_2 and CoS_2 .

The magnetic transition that takes place on going from FeS_2 to CoS_2 allows access to a large range of spin polarizations [6], making this possibly the best studied transition in the pyrite disulfides family. In early experiments, ferromagnetism was found already at very low doping levels of less than x = 0.01 in $\text{Fe}_{1-x}\text{Co}_x\text{S}_2$ [69], an observation that has been confirmed by many later experiments [6, 40, 52] (see experimental points in figure 2).

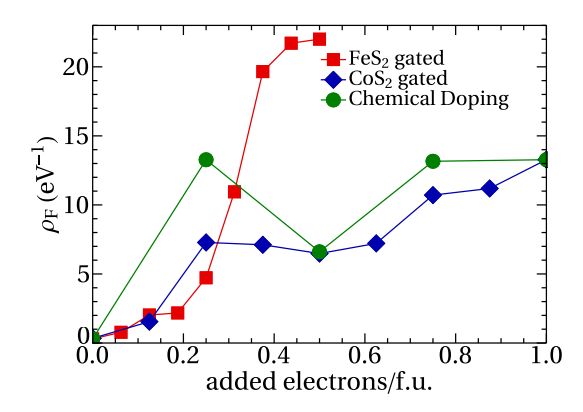


FIG. 3. Calculated density of states at the Fermi level ρ_F as function of the number of added electrons for electrostatically gated FeS₂ (red squares) and CoS₂ (blue diamonds), and chemically doped Fe_{1-x}Co_xS₂ (green circles).

Magnetization measurements show that $Fe_{1-x}Co_xS_2$ is a nearly perfect half-metal across a large range of doping concentrations ($x \approx 0.1 - 0.6$).

First-principles calculations predict ferromagnetism at a larger value $x \approx 0.10-0.15$, and a half-metal with 100% spin polarization emerging at and above $x \approx 0.20 - 0.25$ [60, 61]. These results for the magnetization (open square and circles), combined with our own DFT+U results for chemically doped Fe_{1-x}Co_xS₂ (green circles), are shown in Fig. 2. In agreement with previous results, we find a ferromagnetic transition occurring for 0 < x < 0.25. In contrast, in the case of electrostatically gated FeS₂ (red squares), ferromagnetism onsets only at larger carrier concentrations, equivalent to $x \approx 0.20 - 0.30$, with half-metallicity appearing only at $x \approx 0.40$. Conversely, starting from CoS₂ and adding holes (blue diamonds), half-metallicity starts disappearing around $1 - x \approx 0.4$. The reasons for these differences will be explored in the next subsections, were we contrast the band structure and crystal structure parameters in the cases of chemical doping and electrostatic gating.

B. Density of States

To shed light on the origin of the ferromagnetic state, we plot in Fig. 3 the DOS at the Fermi level, ρ_F , as function of the added carrier concentration. Comparison with the behavior of the magnetization in Fig. 2 suggests that a Stoner mechanism is likely at play [60]. Indeed, at low carrier concentrations, the CD material has a higher DOS at the Fermi level than the EG material, consistent with the fact that the former is ferromagnetic at low doping levels. Similarly, the DOS of the EG materials show a significant increase around $x \approx 0.25$, which coincides with the onset of ferromagnetism in Fig. 2.

The key difference between EG and CD compounds is which bands are being filled. Figure 4(a) shows a schematic representation of the density of states for EG FeS₂, whereas the calculated DOS is shown in Fig. 5(a). The valence band consists of fully occupied t_{2g} orbitals, and the conduction band consists of unoccupied e_g states surrounded by a wide sulfur p-band [70]. This wide band has sulfur-sulfur antibonding character, as shown in Fig. 4(b) [71]. Gating affects the relative bandwidth of the sulfur bands, which decreases for increasing x. Introducing electrons to FeS₂ initially fills this sulfur band, which has a low density of states. Fe e_g states start being occupied only after around 0.25 electrons per iron are added. Once the e_g band starts being filled, the DOS increases significantly, and ferromagnetism emerges. This qualitative picture also applies to EG CoS₂, although it has a narrower sulfur bandwidth as compared to EG FeS₂.

The DOS evolution with carrier concentration is rather different in the case of CD $Fe_{1-x}Co_xS_2$. The reason is because, in the 2+ valence state, iron is slightly more electronegative than cobalt (1.390 vs 1.377 in the scale defined by Yuan et al. [72]), which means that the same electronic orbitals will be at lower energies in cobalt relative to iron. As a result, occupied Co \boldsymbol{e}_g states are lower than the unoccupied e_g states of Fe. These states, which have a large DOS, make up the lower edge of the conduction band as illustrated schematically in Fig. 4(c) and shown quantitatively in Fig. 5(b). Thus, in contrast to the electrostatically gated case, where the added electrons start by occupying low DOS sulfur states, the extra electrons in $\mathrm{Fe_{1-x}Co_xS_2}$ occupy high DOS cobalt e_q states immediately. This is related to the appearance of ferromagnetism at a much lower added carrier concentration.

C. Crystal Structure

The changes in the electronic structure discussed above are also accompanied by changes in the crystal structure, highlighting the importance of effects beyond a simple rigid-band shift in the case of electrostatically gated compounds. Figure 6 shows the evolution of the crystal structure with increasing electron count, contrasting the cases of electrostatic gating (red and blue curves) and chemical doping (green curves). The former is modeled either as electrons added to the FeS₂ structure (red) or as holes added to the CoS_2 compound (blue). There are noticeable changes in the trends of multiple structural parameters near 0.25–0.30 added electrons per formula unit (f.u.). While some changes might seem unphysically large, we emphasize that large values of added carriers are not experimentally feasible via electrostatic gating, and are only included here to illustrate the trends.

These effects are mainly driven by the Fermi level entering the e_g bands at this doping, as discussed in the previous subsection. For less than 0.25 added electrons per f.u., the states that are being filled have sulfur antibonding character, which causes the sulfur-sulfur distance to increase (panel (b)). Once 0.25 electrons per f.u. are added, the e_g bands begin filling, which is reflected in

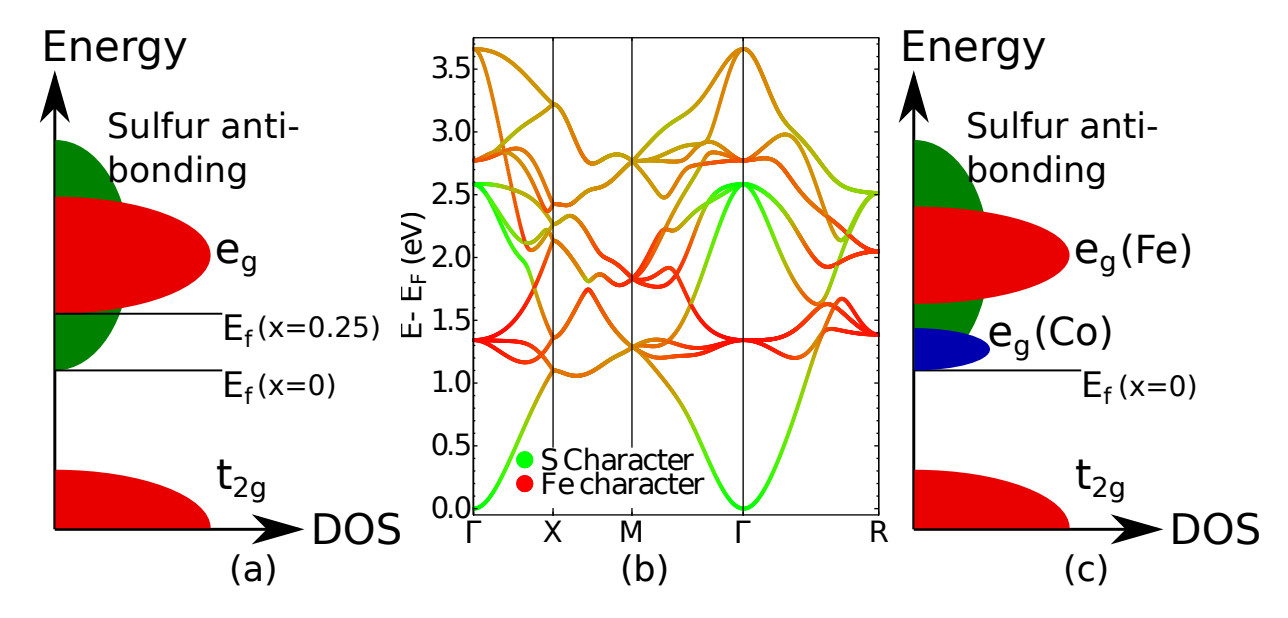


FIG. 4. (a) Schematic representation of the DOS for electrostatic gated FeS₂. The red (green) bands are iron (sulfur) bands. (b) DFT band structure of FeS₂, with red denoting greater iron character and green, greater sulfur character. (c) Schematic representation of the DOS for chemically doped $Fe_{1-x}Co_xS_2$. A cobalt d-band (blue) emerges at the bottom of the wide sulfur band.

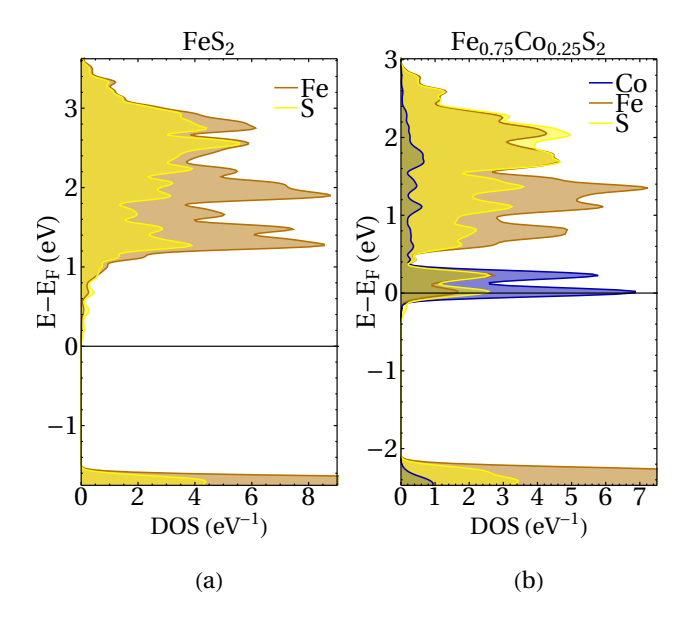


FIG. 5. Calculated densities of states for (a) pure FeS_2 and (b) chemically doped $Fe_{0.75}Co_{0.25}S_2$. The character of the bands are colored according to the legends. Note the prominent peak originating from the Co orbitals at the bottom of the conduction band in the doped case.

the sharp upturn in the transition metal-sulfur distance in the case of FeS_2 (panel (a)). In the case of CoS_2 , there is a much less steep change, although an increase is also observed. At the same time, since there are still some sulfur-sulfur antibonding states at the Fermi level, the lattice constant increases at a faster rate (panel (d)) to compensate for the effects of the internal parameter

u (panel (c)). This behavior of the lattice constant under electrostatic gating strongly deviates from a linear interpolation that would be expected from Vegard's law [73], which is well followed under chemical doping. Indeed, adding 0.25 electrons per Fe increases the lattice constant by more than 4%, whereas 25% Co doping only changes the lattice constant by $\approx .5\%$.

These two effects impact the evolution of the internal parameter u, shown in panel (c). This parameter and the lattice constant a are related to the sulfur-sulfur and metal-sulfur distances as $d_{\rm S-S}=a\sqrt{3}(1-2u)$ and $d_{\rm TM-S}=a\sqrt{\frac{1}{2}-2u+3u^2}$. For these values of u there is a tradeoff: higher u gives a larger transition metal-sulfur distance but a smaller sulfur-sulfur distance. These competing effects lead to the clear non-monotonic behavior of u. For less than 0.25 added electrons per f.u. the effect on the sulfur-sulfur distance is more important, and u decreases. However, for larger numbers of added electrons, once the e_g states begin filling, the transition metal-sulfur distance becomes more important and u increases.

IV. TIGHT-BINDING MODEL

While DFT is able to determine the ground state energy of a specific magnetic configuration, testing all possible types of magnetic order to find the lowest energy state is infeasible. Instead, to screen the possible magnetic wave-vectors, we compute the non-interacting magnetic susceptibility via the Lindhard function. In a weakly interacting system, which should describe doped FeS₂, this quantity provides a good indicator of the different instabilities of the system. While more sophisticated calcula-

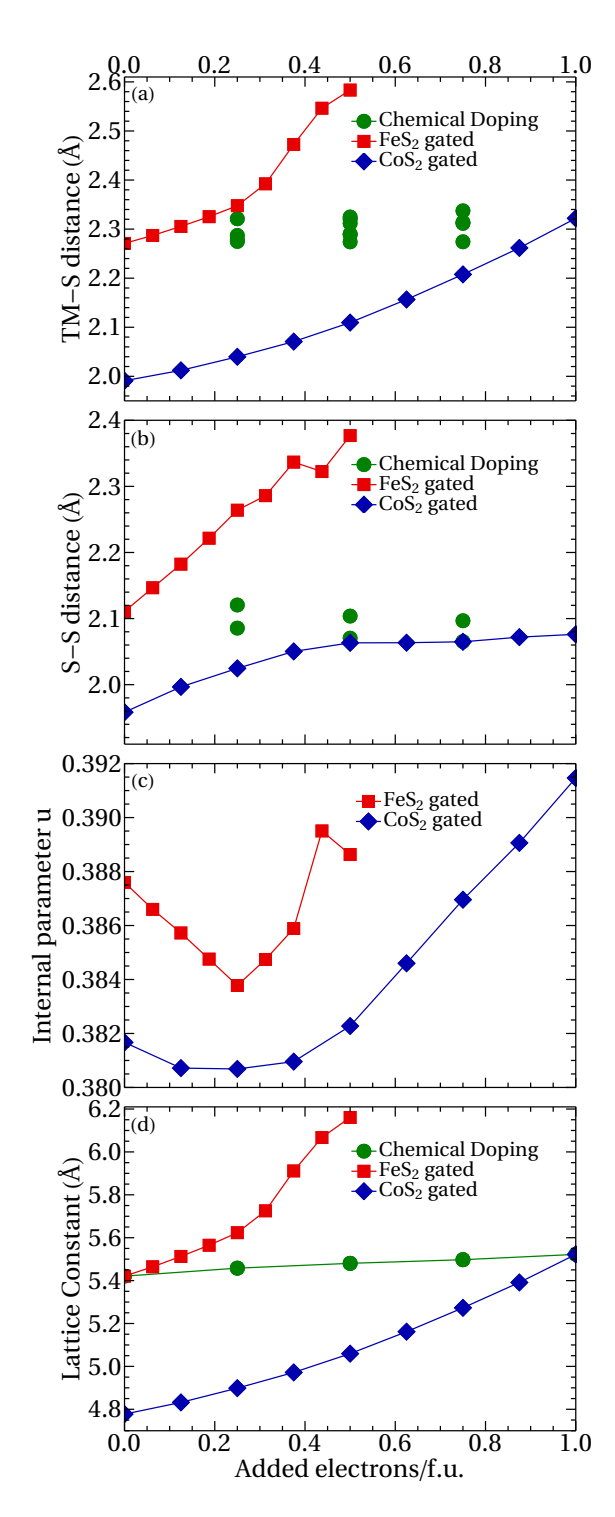


FIG. 6. Plots of several structural parameters as a function of added electrons (per formula unit) for electrostatically-gated FeS_2 (red), electrostatically-gated CoS_2 (blue, in which case the added carriers are actually holes), and chemically doped $\text{Fe}_{1-x}\text{Co}_x\text{S}_2$ (green). The panels display (a) the sulfur-sulfur distance, (b) the transition metal-sulfur distance, (c) the internal sulfur parameter u, and (d) the lattice constant. Chemical doping reduces the symmetry and leads to multiple different TM–S and S–S distances, which are shown as separate datapoints in panels (a) and (b)

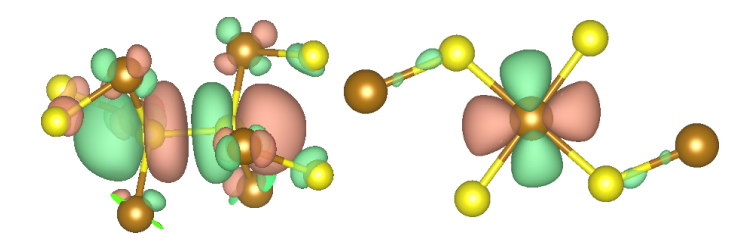


FIG. 7. Illustration of the sulfur-dimer centered Wannier function (left) and transition metal centered Wannier function (right). The sulfur-dimer function has p anti-bonding character, which is the character of the wide band at the bottom of the conduction band shown in Fig. 4(a).

tions that account for electronic interactions are possible, for the scope of this work it suffices to consider the noninteracting susceptibility.

To efficiently compute the Lindhard function, we first construct a tight-binding model from the Wannier functions, which are obtained from a unitary transformation of the Bloch wavefunctions into a new basis. The resulting functions are maximally spatially localized and entirely real [74]. In practice, we calculate an approximate unitary transformation that minimizes the real space spread of the wavefunctions. This additionally gives a maximum ratio of the real and imaginary parts of the wavefunction of less than 10^{-5} . Wannier models are regularly used to interpolate band structures [75], to map Fermi surfaces [76], and to calculate Fermi surface integrals [77]. Figure 7 shows an example of a Wannier function centered on a sulfur dimer with some hybridization to the six transition metal atoms neighboring the sulfur dimer. The other Wannier functions have well-localized e_q character on the transition metal atoms, as also shown in Fig. 7. This Wannier function further emphasizes the covalency between the S atoms in dimers, since the function is centered at the bond center and not on an individual S ion. These dimer orbitals are important to the overall band structure, as discussed above. The entire conduction manifold that consists of the transition metal e_q and sulfur anti-bonding states is used for our Wannier calculations, generating twelve Wannier functions per cell, with no need for disentanglement.

These functions allow us to efficiently derive a tight-binding model of the form:

$$H = \sum_{\vec{R},st} t_{st}^{\vec{R}} \left(\hat{c}_{\vec{R},s}^{\dagger} \hat{c}_{\vec{0},t} + \text{c.c.} \right). \tag{1}$$

from the Wannier basis, where $\hat{c}^{\dagger},\hat{c}$ are creation and annihilation operators, \vec{R} is the vector connecting the unit cells of two orbitals, and s,t are orbital indices within a cell (spin indices are omitted for simplicity). The hopping terms $t_{st}^{\vec{R}} = \langle \vec{0}s|\hat{H}|\vec{R}t\rangle$ are directly computed as the matrix element between the s^{th} Wannier function in the home cell and the t^{th} Wannier function in the cell at \vec{R} . Because we are not interested in finding a minimal model,

twenty distinct hopping vectors are kept corresponding to approximately 700 separate terms. This large number of terms allows us to obtain almost exact agreement with the DFT band structure for all bands (see the supplemental materials for all DFT and tight binding bandstructures). With this model we can very efficiently compute energies at arbitrary k-points.

From the tight-binding model we calculate the magnetic susceptibility in the first Brillouin zone by computing the Lindhardt function. The general non-interacting magnetic susceptibility is given by [78]

$$\chi_{st}^{pq}(\mathbf{q},\omega) = -\frac{1}{N_{\mathbf{k},\mu\nu}} \sum_{\mathbf{k},\mu\nu} \frac{a_{\mu}^{s}(\mathbf{k}) a_{\nu}^{p*}(\mathbf{k} + \mathbf{q}) a_{\nu}^{t*}(\mathbf{k} + \mathbf{q})}{\omega + E_{\nu}(\mathbf{k} + \mathbf{q}) - E_{\mu}(\mathbf{k}) + i0^{+}} \quad (2)$$
$$\times [f(E_{\nu}(\mathbf{k} + \mathbf{q})) - f(E_{\mu}(\mathbf{k}))],$$

where $a_{\mu}^{s}(\mathbf{k})$ are the matrix elements corresponding to the change from orbital basis (latin indices) to band basis (greek indices), $E_{\mu}(\mathbf{k})$ is the energy of band μ at momentum \mathbf{k} , and N is the number of sites. The static susceptibility is [78]

$$\chi^0(\mathbf{q}) = \frac{1}{2} \sum_{sp} \chi_{ss}^{pp}(\mathbf{q}, 0). \tag{3}$$

Figure 8 shows the susceptibilities for EG FeS_2 and CoS_2 , as well as for CD $Fe_{1-x}Co_xS_2$. In agreement with the spin-polarized DFT calculations, we observe a sharp increase in the magnetic susceptibility at the Γ point (i.e. $\mathbf{q} = 0$) starting at 0.25 added electrons per f.u. in both gated compounds, consistent with a tendency towards ferromagnetism. Note that $\chi_0(\Gamma)$ is proportional to the density of states at the Fermi level; thus, the nonmonotonic behavior of the magnitude of $\chi(q)$ as function of doping in the case of CD $Fe_{1-x}Co_xS_2$ is consistent with the non-monotonic dependence of the DOS shown in Fig. 3. The key point of this calculation is to show that, when ferromagnetism emerges upon adding 0.25 electrons per formula unit, the non-interacting susceptibility displays no competing peaks at other wave-vectors. This makes it less likely that competing magnetic states are realized in this compound and, moreover, lends support to the proposal that the ferromagnetism is of Stoner-type.

V. CONCLUSIONS

We performed first principles calculations for both chemically doped ${\rm Fe_{1-x}Co_xS_2}$ and electrostatically gated ${\rm FeS_2}$ and ${\rm CoS_2}$ to elucidate how these different ways of changing the carreir concentration affect the magnetic and electronic properties of these pyrite compounds. We found that electrostatic gating requires a larger concentration of added electrons to induce ferromagnetism as compared to chemical doping. We attribute this behavior to the Stoner nature of the ferromagnetic instability, combined with the fundamentally different ways in

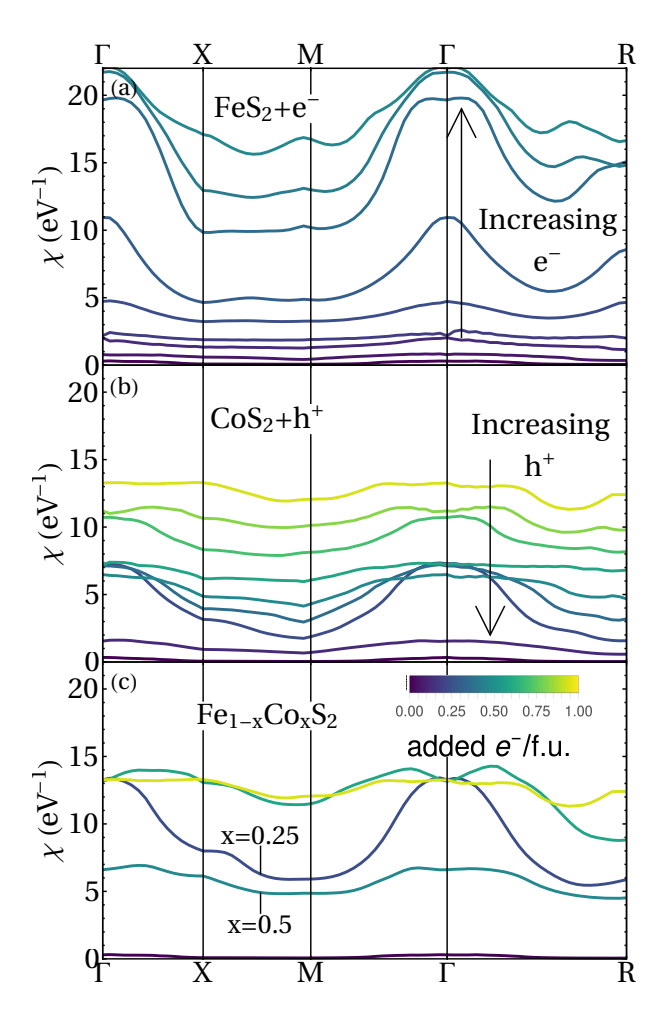


FIG. 8. Non-interacting magnetic susceptibilities in momentum space $\chi(q)$ for (a)gated FeS₂, (b) gated CoS₂, and (c) doped Fe_{1-x}Co_xS₂. Note how in (c) the overall magnitude of the curves is not monotonic with doping.

which the band structure changes upon gating versus doping. Specifically, while Co e_g bands with large DOS form at the bottom of the conduction band when FeS₂ is doped with Co, these bands are not present in electrostatically gated FeS₂. Instead, in the latter case, a low DOS wide sulfur band must first be occupied before the e_g Fe band becomes filled, thus delaying the onset of ferromagnetism.

Our structural relaxation calculations revealed significant changes in several relevant crystalline parameters upon adding electrons via gating. This result demonstrates that electrostatic gating has a much richer impact beyond a rigid-band shift, altering both the crystal structure and the electronic structure. Finally, our tight-binding parametrization allowed us to compute the non-interacting magnetic susceptibility, which revealed a sharp peak at the Γ point consistent with a leading ferromagnetic Stoner-like instability.

Our investigation shows that, even without considering the impact of disorder introduced by dopants, elec-

trostatic gating and chemical doping can affect the electronic properties of a compound in rather different ways, resulting in distinct macroscopic properties. This also suggests that a combination of electrostatic gating and chemical doping may provide an interesting and efficient way to probe and tune electronic ground states. We note that the current capabilities of ionic liquid or gel gating of adding $10^{14} {\rm cm}^{-2}$ would correspond to adding ≈ 0.3 electrons per formula unit in the case of FeS₂ (assuming a penetration depth of one unit cell). Thus, our results suggest that electrolyte gating is a viable means to induce ferromagnetism in FeS₂ purely electrostatically.

ACKNOWLEDGMENTS

We thank Chris Leighton and Jeff Walter for useful discussions. This work was supported by the National Science Foundation through the UMN MRSEC under DMR-1420013. The authors acknowledge the Minnesota Supercomputing Institute (MSI) at the University of Minnesota for providing resources that contributed to the research results reported within this paper.

- S. Ogawa, Journal of the Physical Society of Japan 41, 462 (1976).
- [2] T. Chattopadhyay, P. Burlet, and P. J. Brown, Journal of Physics: Condensed Matter 3, 5555 (1991).
- [3] M. Lin and H. Hacker, Solid State Communications 6, 687 (1968).
- [4] S. A. J. Kimber and T. Chatterji, Journal of Physics: Condensed Matter 27, 226003 (2015).
- [5] G. L. Zhao, J. Callaway, and M. Hayashibara, Phys. Rev. B 48, 15781 (1993).
- [6] C. Leighton, M. Manno, A. Cady, J. W. Freeland, L. Wang, K. Umemoto, R. M. Wentzcovitch, T. Y. Chen, C. L. Chien, P. L. Kuhns, M. J. R. Hoch, A. P. Reyes, W. G. Moulton, E. D. Dahlberg, J. Checkelsky, and J. Eckert, Journal of Physics: Condensed Matter 19, 315219 (2007).
- [7] M. Matsuura, Y. Endoh, H. Hiraka, K. Yamada, A. S. Mishchenko, N. Nagaosa, and I. V. Solovyev, Phys. Rev. B 68, 094409 (2003).
- [8] C. Schuster, M. Gatti, and A. Rubio, The European Physical Journal B 85, 325 (2012).
- [9] S. Yano, D. Louca, J. Yang, U. Chatterjee, D. E. Bugaris, D. Y. Chung, L. Peng, M. Grayson, and M. G. Kanatzidis, Phys. Rev. B 93, 024409 (2016).
- [10] T. Bither, C. Prewitt, J. Gillson, P. Bierstedt, R. Flippen, and H. Young, Solid State Communications 4, 533 (1966).
- [11] H. Ueda, M. Nohara, K. Kitazawa, H. Takagi, A. Fujimori, T. Mizokawa, and T. Yagi, Phys. Rev. B 65, 155104 (2002).
- [12] D. W. Bullett, Journal of Physics C: Solid State Physics 15, 6163 (1982).
- [13] A. Goldman, Annu. Rev. Mater. Res. 44, 45 (2014).
- [14] J. D. Burton and E. Y. Tsymbal, Physical Review Letters 107, 166601 (2011).
- [15] X. Liu, E. Y. Tsymbal, and K. M. Rabe, Physical Review B 97, 094107 (2018).
- [16] H.-T. Zhang, Z. Zhang, H. Zhou, H. Tanaka, D. D. Fong, and S. Ramanathan, Advances in Physics: X 4, 1523686 (2019).
- [17] C. Song, B. Cui, J. Peng, H. Mao, and F. Pan, Chinese Physics B 25, 067502 (2016).
- [18] R. Scherwitzl, P. Zubko, I. G. Lezama, S. Ono, A. F. Morpurgo, G. Catalan, and J.-M. Triscone, Advanced Materials 22, 5517 (2010).

- [19] K. Ueno, S. Nakamura, H. Shimotani, A. Ohtomo, N. Kimura, T. Nojima, H. Aoki, Y. Iwasa, and M. Kawasaki, Nature Materials 7, 855 (2008).
- [20] J. Jeong, N. Aetukuri, T. Graf, T. D. Schladt, M. G. Samant, and S. S. P. Parkin, Science 339, 1402 (2013).
- [21] S. Z. Bisri, S. Shimizu, M. Nakano, and Y. Iwasa, Advanced Materials 29, 1607054 (2017).
- [22] H. Yuan, H. Shimotani, A. Tsukazaki, A. Ohtomo, M. Kawasaki, and Y. Iwasa, Advanced Functional Materials 19, 1046 (2009).
- [23] J. Jeong, N. B. Aetukuri, D. Passarello, S. D. Conradson, M. G. Samant, and S. S. P. Parkin, Proceedings of the National Academy of Sciences 112, 1013 (2015).
- [24] D. Okuyama, M. Nakano, S. Takeshita, H. Ohsumi, S. Tardif, K. Shibuya, T. Hatano, H. Yumoto, T. Koyama, H. Ohashi, M. Takata, M. Kawasaki, T. Arima, Y. Tokura, and Y. Iwasa, Applied Physics Letters 104, 023507 (2014).
- [25] C. J. Dahlman, G. LeBlanc, A. Bergerud, C. Staller, J. Adair, and D. J. Milliron, Nano Letters 16, 6021 (2016).
- [26] H. T. Yi, B. Gao, W. Xie, S.-W. Cheong, and V. Podzorov, Scientific Reports 4, 6604 (2014).
- [27] S. Shimizu, K. S. Takahashi, M. Kubota, M. Kawasaki, Y. Tokura, and Y. Iwasa, Applied Physics Letters 105, 163509 (2014).
- [28] S. Shimizu, S. Ono, T. Hatano, Y. Iwasa, and Y. Tokura, Phys. Rev. B 92, 165304 (2015).
- [29] A. T. Bollinger, G. Dubuis, J. Yoon, D. Pavuna, J. Misewich, and I. Bozovic, Nature 472, 458 (2011).
- [30] X. Leng, J. Garcia-Barriocanal, S. Bose, Y. Lee, and A. M. Goldman, Phys. Rev. Lett. 107, 027001 (2011).
- [31] J. T. Ye, Y. J. Zhang, R. Akashi, M. S. Bahramy, R. Arita, and Y. Iwasa, Science 338, 1193 (2012).
- [32] T. A. Petach, M. Lee, R. C. Davis, A. Mehta, and D. Goldhaber-Gordon, Phys. Rev. B 90, 081108 (2014).
- [33] S. Bubel, A. J. Hauser, A. M. Glaudell, T. E. Mates, S. Stemmer, and M. L. Chabinyc, Applied Physics Letters 106, 122102 (2015).
- [34] C. Leighton, Nature Materials 18, 13 (2019).
- [35] J. Walter, G. Yu, B. Yu, A. Grutter, B. Kirby, J. Borchers, Z. Zhang, H. Zhou, T. Birol, M. Greven, and C. Leighton, Phys. Rev. Materials 1, 071403 (2017).
- [36] F. Chen, Q. Qing, J. Xia, J. Li, and N. Tao, Journal of the American Chemical Society 131, 9908 (2009).

- [37] H. Yuan, H. Shimotani, J. Ye, S. Yoon, H. Aliah, A. Tsukazaki, M. Kawasaki, and Y. Iwasa, Journal of the American Chemical Society 132, 18402 (2010).
- [38] N. J. Kay, S. J. Higgins, J. O. Jeppesen, E. Leary, J. Lycoops, J. Ulstrup, and R. J. Nichols, Journal of the American Chemical Society 134, 16817 (2012).
- [39] C. Ge, K.-J. Jin, L. Gu, L.-C. Peng, Y.-S. Hu, H.-Z. Guo, H.-F. Shi, J.-K. Li, J.-O. Wang, X.-X. Guo, C. Wang, M. He, H.-B. Lu, and G.-Z. Yang, Advanced Materials Interfaces 2, 1500407 (2015).
- [40] K. Ramesha, R. Seshadri, C. Ederer, T. He, and M. A. Subramanian, Phys. Rev. B 70, 214409 (2004).
- [41] R. Sun, M. K. Y. Chan, S. Y. Kang, and G. Ceder, Physical Review B 84, 035212 (2011).
- [42] Ray, Voigt, Manno, Leighton, Aydil, and Gagliardi, Under Review.
- [43] P. P. Altermatt, T. Kiesewetter, K. Ellmer, and H. Tributsch, Solar Energy Materials and Solar Cells 71, 181 (2002).
- [44] Y. Bi, Y. Yuan, C. L. Exstrom, S. A. Darveau, and J. Huang, Nano Letters 11, 4953 (2011).
- [45] F. Alharbi, J. D. Bass, A. Salhi, A. Alyamani, H.-C. Kim, and R. D. Miller, Renewable Energy 36, 2753 (2011).
- [46] K. Umemoto, R. M. Wentzcovitch, L. Wang, and C. Leighton, physica status solidi (b) 243, 2117 (2006).
- [47] B. Voigt, W. Moore, M. Manno, J. Walter, J. D. Jeremiason, E. S. Aydil, and C. Leighton, ACS Applied Materials and Interfaces 11, 15552 (2019).
- [48] M. Limpinsel, N. Farhi, N. Berry, J. Lindemuth, C. L. Perkins, Q. Lin, and M. Law, Energy and Environmental Science 7, 1974 (2014).
- [49] D. Liang, M. Cabán-Acevedo, N. S. Kaiser, and S. Jin, Nano Letters 14, 6754 (2014).
- [50] X. Zhang, M. Li, J. Walter, L. O'Brien, M. A. Manno, B. Voigt, F. Mork, S. V. Baryshev, J. Kakalios, E. S. Aydil, and C. Leighton, Phys. Rev. Materials 1, 015402 (2017).
- [51] J. Walter, X. Zhang, B. Voigt, R. Hool, M. Manno, F. Mork, E. S. Aydil, and C. Leighton, Phys. Rev. Materials 1, 065403 (2017).
- [52] S. Guo, D. P. Young, R. T. Macaluso, D. A. Browne, N. L. Henderson, J. Y. Chan, L. L. Henry, and J. F. DiTusa, Phys. Rev. Lett. 100, 017209 (2008).
- [53] S. Guo, D. P. Young, R. T. Macaluso, D. A. Browne, N. L. Henderson, J. Y. Chan, L. L. Henry, and J. F. DiTusa, Phys. Rev. B 81, 144423 (2010).
- [54] M. Kotiuga and K. M. Rabe, "High-density electron doping of smnio₃ from first principles," (2019), arXiv:1909.03425 [cond-mat.mes-hall].
- [55] G. Kresse and J. Furthmüller, Phys. Rev. B 54, 11169 (1996).

- [56] G. Kresse and D. Joubert, Phys. Rev. B 59, 1758 (1999).
- [57] J. P. Perdew, A. Ruzsinszky, G. I. Csonka, O. A. Vydrov, G. E. Scuseria, L. A. Constantin, X. Zhou, and K. Burke, Phys. Rev. Lett. 100, 136406 (2008).
- [58] S. L. Dudarev, G. A. Botton, S. Y. Savrasov, C. J. Humphreys, and A. P. Sutton, Phys. Rev. B 57, 1505 (1998).
- [59] J. Hu, Y. Zhang, M. Law, and R. Wu, Phys. Rev. B 85, 085203 (2012).
- [60] I. I. Mazin, Applied Physics Letters 77, 3000 (2000).
- [61] Z.-Y. Feng, Y. Yang, and J.-M. Zhang, Materials Research Express 5, 016507 (2018).
- [62] A. A. Mostofi, J. R. Yates, G. Pizzi, Y.-S. Lee, I. Souza, D. Vanderbilt, and N. Marzari, Computer Physics Communications 185, 2309 (2014).
- [63] As is standard in similar DFT calculations, a homogeneous background charge is also added to ensure charge neutrality of the unit cell.
- [64] I. Souza, N. Marzari, and D. Vanderbilt, Phys. Rev. B 65, 035109 (2001).
- [65] S. L. Finklea, III, L. Cathey, and E. L. Amma, Acta Crystallographica Section A 32, 529 (1976).
- [66] D. Lundqvist and A. Westgren, Zeitschrift für anorganische und allgemeine Chemie 239, 85 (1938).
- [67] E. Nowack, D. Schwarzenbach, and T. Hahn, Acta Crystallographica Section B 47, 650 (1991).
- [68] S. S. Streltsov, A. O. Shorikov, S. L. Skornyakov, A. I. Poteryaev, and D. I. Khomskii, Scientific Reports 7, 13005 (2017).
- [69] H. S. Jarrett, W. H. Cloud, R. J. Bouchard, S. R. Butler, C. G. Frederick, and J. L. Gillson, Physical Review Letters 21, 617 (1968).
- [70] V. Eyert, K.-H. Höck, S. Fiechter, and H. Tributsch, Phys. Rev. B 57, 6350 (1998).
- [71] W. Folkerts, G. A. Sawatzky, C. Haas, R. A. de Groot, and F. U. Hillebrecht, Journal of Physics C: Solid State Physics 20, 4135 (1987).
- [72] K. Li and D. Xue, The Journal of Physical Chemistry A 110, 11332 (2006).
- [73] L. Vegard, Zeitschrift für Physik 5, 17 (1921).
- [74] N. Marzari, A. A. Mostofi, J. R. Yates, I. Souza, and D. Vanderbilt, Rev. Mod. Phys. 84, 1419 (2012).
- [75] A. Ramasubramaniam, Phys. Rev. B 86, 115409 (2012).
- [76] C. Shekhar, A. K. Nayak, Y. Sun, M. Schmidt, M. Nick-las, I. Leermakers, U. Zeitler, Y. Skourski, J. Wosnitza, Z. Liu, Y. Chen, W. Schnelle, H. Borrmann, Y. Grin, C. Felser, and B. Yan, Nature Physics 11, 645 (2015).
- [77] J. R. Yates, X. Wang, D. Vanderbilt, and I. Souza, Phys. Rev. B 75, 195121 (2007).
- [78] S. Graser, T. A. Maier, P. J. Hirschfeld, and D. J. Scalapino, New Journal of Physics 11, 025016 (2009).